Solid Earth, 8, 943–953, 2017
https://doi.org/10.5194/se-8-943-2017

Solid Earth Open Access EGU

Strain field evolution at the ductile-to-brittle transition: a case study on ice

Thomas Chauve[1], **Maurine Montagnat**[1], **Cedric Lachaud**[1], **David Georges**[1], **and Pierre Vacher**[2]

[1]Université Grenoble Alpes, CNRS, IRD, G-INP, IGE, 38041 Grenoble, France
[2]Laboratoire SYMME, Université de Savoie Mont Blanc, BP 80439, 74944 Annecy le Vieux CEDEX, France

Correspondence to: M. Montagnat (maurine.montagnat@univ-grenoble-alpes.fr)

Received: 27 February 2017 – Discussion started: 17 March 2017
Revised: 20 June 2017 – Accepted: 7 August 2017 – Published: 18 September 2017

Abstract. This paper presents, for the first time, the evolution of the local heterogeneous strain field around intra-granular cracking in polycrystalline ice, at the onset of tertiary creep. Owing to the high homologous temperature conditions and relatively low compressive stress applied, stress concentration at the crack tips is relaxed by plastic mechanisms associated with dynamic recrystallization. Strain field evolution followed by digital image correlation (DIC) directly shows the redistribution of strain during crack opening, but also the redistribution driven by crack tip plasticity mechanisms and recrystallization. Associated local changes in microstructure induce modifications of the local stress field evidenced by crack closure during deformation. At the ductile-to-brittle transition in ice, micro-cracking and dynamic recrystallization mechanisms can co-exist and interact, the later being efficient to relax stress concentration at the crack tips.

1 Introduction

The evaluation and the characterization of strain heterogeneities is of primary importance in material sciences at various scales of observation. Plastic strain localization in metals plays a crucial role on the propagation of fracture and on the response to fatigue conditions, and Portevin-Le-Chatelier is a strong example of plastic strain heterogeneities development during mechanical tests in some metal alloys (see Antolovich and Armstrong, 2014, for a review). Similarly, strain heterogeneities and localization are known to strongly influence the rheological behavior of the Earth lithosphere, in particular to explain post-seismic deformation (Tommasi et al., 2009; Vauchez et al., 2012).

In the context of ice sheet flow, successive layers of ice with slightly different viscosity can experience different strain history as a result of strain localization initiated by bedrock topography (Paterson, 1994; Durand et al., 2004, 2007). Strain localization can induce flow disturbances that can mix the climatic signal and counteract the search for the oldest ice (Dahl-Jensen et al., 2013; Fischer et al., 2013). These flow disturbances can form as folding that is observed at large scale from ice-penetrating radar surveys now able to highlight deep stratigraphy (MacGregor et al., 2015; Panton and Karlsson, 2015; Bons et al., 2016), but also at smaller scales from microstructure observations (Jansen et al., 2016).

During ductile deformation of ice in natural or laboratory conditions (at high homologous temperature of $\sim 0.97\ T_m$, low strain rate of $\sim 10^{-7}\mathrm{s}^{-1}$ and low stress of 0.5–1 MPa), plastic deformation is mainly accommodated by the glide of basal dislocations (Duval et al., 1983). The resulting strongly anisotropic viscoplastic behavior of the single crystal leads to the development of strong strain heterogeneities during deformation of polycrystalline ice (Duval et al., 1983).

Strain heterogeneities evaluated during transient creep of ice were shown to reach local values higher than 10 times the macroscopic strain, and to settle into bands whose dimensions are higher than the grain size. Strain localization bands may follow grain boundaries, but they also cross entire grains, and there is no statistical link between the crystallographic orientation and the amount of local strain (Grennerat et al., 2012). These first measurements of strain localization during laboratory experiments were restricted to transient (or primary) creep conditions, in ductile conditions ($\sigma < 0.5$ MPa and $T > 0.97\ T_m$) and prior to any microstructure modification due to dynamic recrystallization.

More generally, creep of isotropic polycrystalline ice is characterized by a three-stage behavior, with a strong decrease in strain rate during primary creep, down to a minimum reached at about 1 % strain, also called secondary creep, immediately followed by a increase in strain rate to reach tertiary creep at about 10 % strain (see Jacka and Maccagnan, 1984; Duval et al., 1983, for instance).

At the onset of tertiary creep, for experiment performed at low strain rate ($< 10^{-7}\,s^{-1}$) or low stress (< 0.5 MPa), dynamic recrystallization mechanisms occur increasingly to relax the kinematic hardening and enable for further ductile deformation to occur (Duval et al., 1983). Dynamic recrystallization leads to strong modification in microstructure and texture (Duval, 1979; Jacka and Maccagnan, 1984; Montagnat et al., 2015) through various mechanisms such as nucleation of new grains or polygonization associated with sub-grain boundaries and bulging, recently characterized by cryo-EBSD (electron backscatter diffraction; Chauve et al., 2017). While Piazolo et al. (2015) showed that sub-grain boundary formation such as kink bands could be correlated with heterogeneities of local stress (simulated with a full-field crystal plasticity code, CraFT), Chauve et al. (2015) were able to directly associate nucleation mechanisms (polygonization, bulging) with local modification of the strain field estimated in situ from digital image correlation (DIC) measurements.

During experiments performed at higher imposed stress (typically above 0.9 MPa), the increase in strain rate after secondary creep can also be associated with the occurrence of micro-cracking without a total collapse of the sample (Schulson et al., 1984; Batto and Schulson, 1993; Schulson and Duval, 2009). The local stress field is therefore relaxed by cracks opening at or close to grain boundaries, and depending on the boundary conditions, crack propagation can occur at various rates. This mechanical response is typical of a ductile-to-brittle transition (Schulson and Buck, 1995; Schulson and Duval, 2009).

In this domain, most of the studies performed so far, some of which are mentioned here, have focused on macroscopic parameters (deformation and creep curves, evaluation of the effect of temperature and grain size on strength) and optical observations of the full sample to characterize the nature of the cracks (Batto and Schulson, 1993; Iliescu and Schulson, 2004). From these observations, a theoretical framework was elaborated based on the assumption of the formation of wing cracks at the tip of initial cracks to relax the local stress field (Renshaw and Schulson, 2001). In particular, the conditions required to form these secondary cracks were shown to control the ductile-to-brittle transition under compression. More recently, Snyder et al. (2016) showed that this model was able to take into account the effect of a pre-strain, including recrystallization mechanisms, on the increase in ductile-to-brittle transition strain rate for ice.

At the ductile-to-brittle transition, mixture of creep by dislocations and cracking will occur, and it is related to the ability of the material to relax the stress accumulated at the tip of the initial cracks. For instance, Batto and Schulson (1993) showed that a small amount of creep relaxation at the crack tip could be enough to postponed the transition to brittle behavior (in time or in strain-rate level). The mechanism of relaxation of the stress produced by a crack opening in mode I through rapid multiplication of dislocations at the crack tip was pioneered by Rice and Thomson (1974) and has been reviewed by Argon (2001) for metallic materials. More recently, Martínez-Pañeda and Niordson (2016) were able to simulate the complexity of the effect of strain gradient plasticity on the level of stress at the crack tip and on crack-tip blunting. Crack-tip-initiated plasticity is a crucial mechanism to explain a ductile-like behavior at the ductile-to-brittle transition.

In the present work we use the DIC technique, already well proven on ice, to evaluate the strain field evolution during a creep experiment on ice polycrystal performed at the ductile-to-brittle transition. After a brief presentation of the experimental setup (Sect. 2), Sect. 3 will explore stress conditions during which strain-rate increase with tertiary creep results from local cracking. We will see that plasticity is strongly active at the crack tips as evidenced by the occurrence of dynamic recrystallization mechanisms. These mechanisms, by modifying the microstructure, indeed play a crucial role to reduce and redistribute the local stress concentration that appears at the crack tips during the ductile-to-brittle transition.

2 Experimental setup

Unconfined uniaxial creep tests have been carried out on polycrystalline columnar ice samples of type S2 (Ple and Meyssonnier, 1997). Parallelepipedic samples ($\sim 90 \times 90 \times 15$ mm) were built and the column axes were positioned perpendicularly to the larger surface, and to the compression axis (Fig. 1). By doing so, the samples provide a "2-D–1/2" microstructure, from which surface characterization satisfactorily reflects volume behavior. Sample microstructure and texture were measured using an automatic ice texture analyzer (AITA; Wilson et al., 2003; Peternell et al., 2011), which is an optical technique measuring the c axis (or optical axis) orientation (azimuth θ and colatitude ϕ) with a spatial resolution from 50 to 5 µm, and an angular resolution of about 3°. Although large areas can be analyzed (up to 120×120 mm), this technique requires the preparation of thin sections of ice (~ 0.3 mm thick), and is then destructive. By taking advantage of the columnar microstructure, we were able to compare pre- and post-deformation microstructures by carefully extracting thin layers of ice before and after the test (Fig. 1). Details of the procedure for sample preparation can be found in Grennerat et al. (2012) and Chauve et al. (2015).

During the experiment, DIC analyses were performed over the full surface of the samples by following the procedure adapted to ice by Grennerat et al. (2012). DIC provides in

Table 1. Characteristics of the DIC measurements.

Camera	DIC spatial resolution	DIC strain resolution		
		$\sigma_{\varepsilon_{xx}}$	$\sigma_{\varepsilon_{yy}}$	$\sigma_{\varepsilon_{xy}}$
Phase One 80 Mpx	0.19 mm pix^{-1}	4.10^{-3}	3.10^{-3}	4.10^{-3}

situ measurements of the displacement and therefore strain field on the sample surface, from the correlation of surface images of a grey-level speckle that follows the sample deformation. By taking advantage of the 2-D–1/2 configuration, we assumed the surface strain field to be as representative as possible of the volume deformation. This configuration makes it possible to compare the microstructures measured by AITA (before and after the test) to the strain field evaluated by DIC (Fig. 1).

The spatial resolution strongly depends on the quality of the speckle, the illumination and the sensitivity of the camera used. In the following experiments, we used a Phase One 80 Mpx camera, the speckle was made of shoe polish that offers good cohesion with the ice surface and good illumination was obtained thanks to two neon lamps. From this, we ended up with a spatial resolution of 0.19 mm pix^{-1}, and a strain resolution between 3.10^{-3} and 4.10^{-3} for the different strain components (see Table 2).

Displacement and total strain data were extracted using the 7-D software from Vacher et al. (1999). This DIC method provides a set of displacement vectors over a given grid, defined for the DIC calculation as a function of the speckle and picture qualities (Vacher et al., 1999). From the displacement field components, the total strain components are extracted by using Green–Lagrange expression. Please note that the elastic and plastic components can not be separated, and strain field refers to the total strain field. In the case of ice, elasticity is very low and nearly isotropic, and can be neglected (Schulson and Duval, 2009). In-plane components of strain are therefore provided (ε_{xx}, ε_{yy} and ε_{xy}), from which an equivalent strain ($\varepsilon_{\mathrm{eq}} = \sqrt{\frac{2}{3}\left(\varepsilon_{xx}^2 + \varepsilon_{yy}^2 + 2\varepsilon_{xy}^2\right)}$) and principal strain components are calculated. The later will be plotted along their principal directions in the following figures.

Discontinuities such as cracks produce displacements whose translation in terms of strain is not direct but could be estimated as shown by Nguyen et al. (2011). In the present study, we simply use the direction of the principal strain components calculated around a crack to interpret the direction of the crack opening (or closing), since the displacement produced is small enough to be followed by the speckle on each side of the crack.

Since all surfaces except the loaded ones remained free (unconfined tests), a limited amount of out-of-plane shear cannot be excluded. The effect of a deformation going out of the plane xOy was estimated in previous analyses performed by Grennerat et al. (2012) and shown to remain low, within

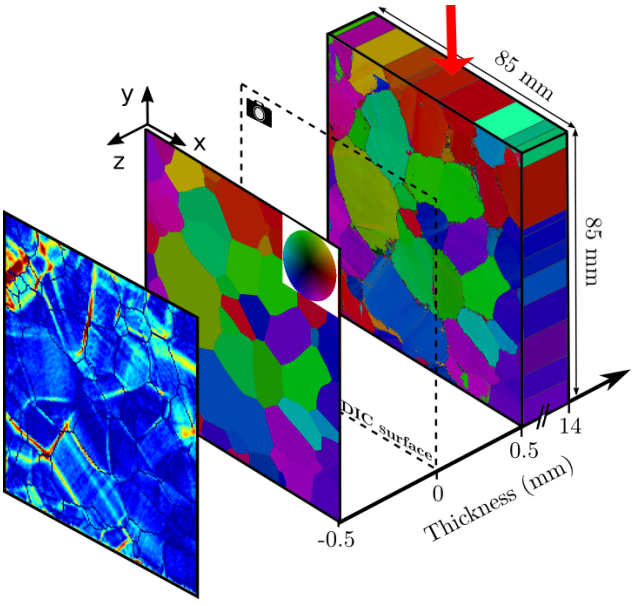

Figure 1. Scheme of the experimental setup showing the shape of the sample with the direction of imposed stress (red arrow). Position 0 corresponds to the sample surface (during the test) on top of which the speckle is marked. The microstructure analyzed by AITA prior to deformation is located at about −0.5 mm and the one after deformation is at about 0.5 mm from the sample surface (0.5 mm corresponds to the ice thickness needed to make the thin section). The strain-field image, measured at position 0, is added in the front plan for illustration.

the limit of the small macroscopic deformations reached in the present study (less than 5.5 %). In order to reduce the noise and this out-of-plane strain effect on the evaluation of the strain evolution during the experiment, we calculated the strain field during short increments of macroscopic deformation of 0.1 to 0.5 %. Additionally, observation of the incremental strain field enables individualizing consecutive events that would be hidden in a strain field calculation integrating the whole experiment duration.

Table 2 summarizes the experimental conditions of the test used as an illustration in this paper, and Fig. 2 provides the creep curves. The minimum strain rate is reached at about 0.5 % of compressive macro-strain, slightly before the standard 1 % value. This can be attributed to a microstructure effect since our 2-D–1/2 samples contain only few grains and do not form good representative volume elements. In the following, a negative sign will be given to the compressive strain, at the macroscopic and local scale.

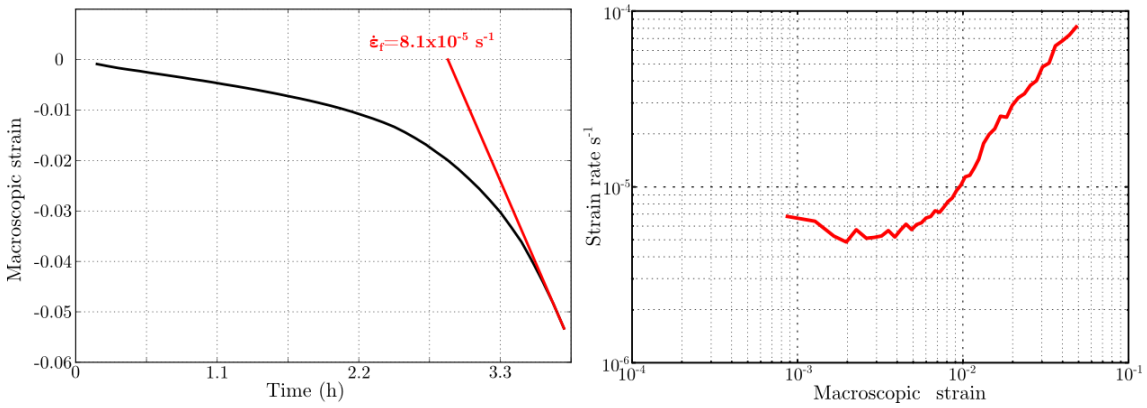

Figure 2. Evolution of the macroscopic strain and strain rate measured by DIC. Values less than 10^{-3} macro-strain were not calculated.

Table 2. Experimental conditions at the ductile-to-brittle transition for the illustrative test presented here. The minimum creep rate is reached at about $-0.5\,\%$ strain.

Stress	Temperature	Strain rate (s^{-1})	
(MPa)	(°C)	mini ($\varepsilon_{yy} = -0.5\,\%$)	end ($\varepsilon_{yy} = -5.5\,\%$)
1.0	−7	5.0×10^{-6}	8.1×10^{-5}

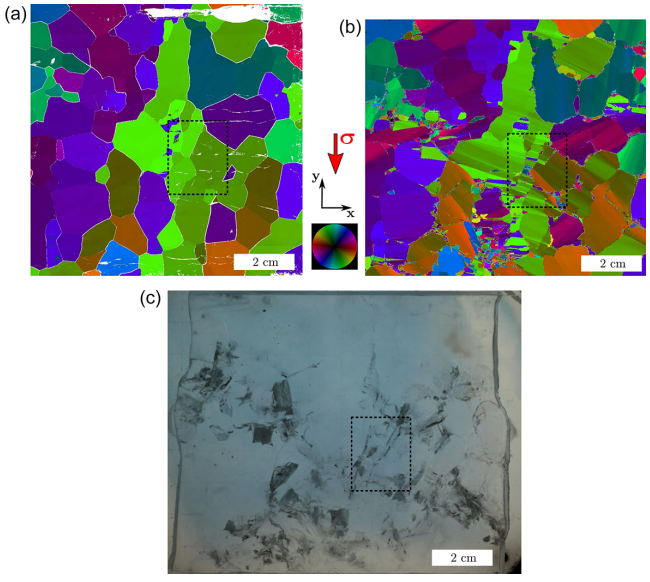

Figure 3. Microstructure (color-coded c axis orientation, from AITA analysis) before deformation **(a)** and after $-5.5\,\%$ of compressive creep at $-7\,°C$ under 1 MPa **(b)**. **(c)** Raw picture of the sample taken in natural light at the end of the compressive test. Black areas result from light diffusion by cracks and de-cohesion features. The dashed black rectangle shows the area studied in detail in the paper.

3 Strain field evolution at the ductile-to-brittle transition

The macroscopic strain curve reveals an increase in strain rate after $-0.5\,\%$ of ε_{yy} (vertical) macro-strain (Fig. 2). At $-0.5\,\%$ of macro-strain the minimum strain rate is $5.0 \times 10^{-6}\,s^{-1}$ and at the end of the experiment the strain rate reaches $8.1 \times 10^{-5}\,s^{-1}$, evidencing an acceleration at the onset of tertiary creep captured here.

The initial microstructure of the sample, the ending one and an optical observation of the full sample at the end of the test are shown in Fig. 3. Thanks to the transparency of ice, cracks and de-cohesion features can be observed with natural light. They appear as grey and black areas in Fig. 3. Both features were clearly distinguished and analyzed by Weiss and Schulson (2000). From the c axis orientation color scale, one can see that the initial texture is not isotropic. On top of the expected columnar grain-shape effect, we therefore expect, as observed (Fig. 2), a macroscopic mechanical response different from the one of an isotropic granular sample.

The global strain field measured prior to any visible crack opening on the speckle, at $-0.5\,\%$ of macro-strain (at the minimum creep rate), is represented in Fig. 4 via the equivalent strain ε_{eq} at two different spatial resolutions in order to illustrate the structure of strain heterogeneities. Similarly to what was already observed by Grennerat et al. (2012), the deformation is organized into bands crossing most of the sample. The main orientation of the bands is about 20 to 30° E from the compression direction. Local equivalent strain amplitude in the deformation bands can reach more than $10\,\%$, for a ε_{yy} macro-strain of about $-0.5\,\%$.

In the following, focus will be given to a small area located within the dashed black rectangle of Fig. 3. The initial microstructure and orientations of the grains in this area, the final microstructure where cracks, sub-grain boundaries and small nucleated grains appear and a picture of the speckle from the surface of the sample where crack locations are visible (arrows 1 to 4) are shown in Fig. 5. Very small grains visible inside the cracks are artifacts from the thin sectioning process (shaving produces small chips that fill the crack in-

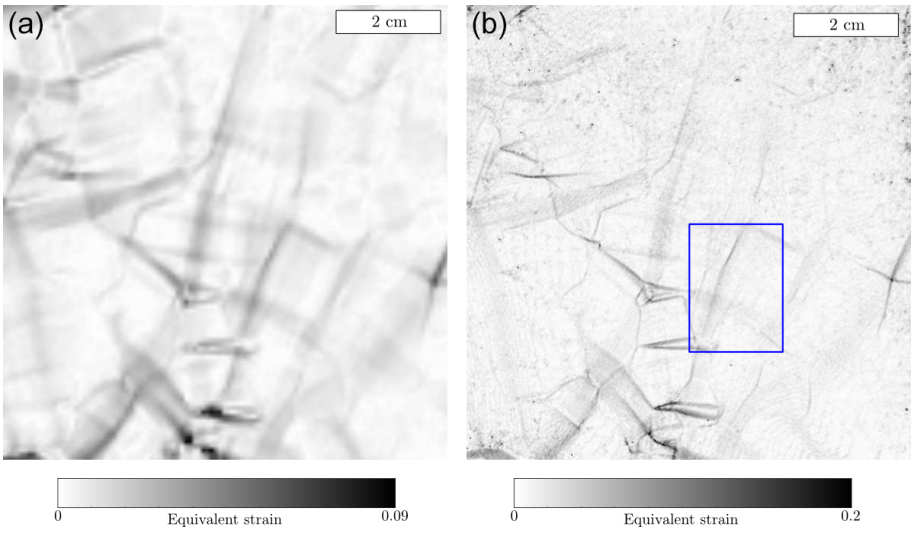

Figure 4. Map of equivalent strain (ε_{eq}) after $-0.47\,\%$ of compressive deformation. The blue rectangle shows the area studied in detail in the paper. **(a)** Spatial resolution of 0.76 mm pix^{-1}. **(b)** Spatial resolution of 0.19 mm pix^{-1}.

terior), but new grains from dynamic recrystallization mechanisms (DRX) can be distinguished away from the crack interior. See for instance the new blue area in between the bottom of crack 2 and top of crack 3. Also the dark blue grain at the bottom of crack 3, and the pink–purple ones surrounding crack 4. None of these new grains were pre-existing in the initial microstructure, therefore illustrating DRX nucleation. Grain boundaries surrounding new small grains can appear more irregular than in reality because of intrinsic limitation of the AITA observation based on thin sections (about 0.3 mm thick). A lot of sub-grain boundaries similar to the tilt and kink bands characterized in Chauve et al. (2015, 2017) are visible after deformation. A tilt band is composed of basal edge dislocations and can accommodate a large misorientation, as observed here. A kink band is composed of two nearby tilt bands that accommodate opposite misorientations. For instance, a highly misoriented tilt band is visible as a sharp transition between orange and light brown close to cracks 2 and 3 (ellipse). Between cracks 2 and 1, the two close color transitions (from green to blue to green, and from brown to green to brown) illustrate misorientations resulting from kink bands.

Intra-granular cracks (cracks 1, 3 and 4) and cracks along grain boundaries (crack 2) are observed. Observed intragranular cracks do not always cross the entire grain, such as crack 1, which seems interrupted in the middle of the grain (Fig. 5). This final microstructure very likely results from strong strain heterogeneities at grain boundaries and within grain interiors.

In the following, we track the history of formation of the four cracks labeled in Fig. 3 by analyzing the strain field evolution through the principal strain components, such as in Chauve et al. (2015). The principal strain component representation enables us to distinguish among the components of the local strain.

Within this area of interest, the deformation before the apparition of any crack is localized in two main bands, one crossing the full area at about 10 to 20° E from the vertical (compression) direction, and another one in the bottom part of the area, nearly perpendicular to the first one (Fig. 6, left). Both bands are following some boundaries and crossing some grains. The principal strain components are typical of a local pure shear configuration.

The accumulated strain field just before (at $\varepsilon_{yy} = -1.35\,\%$), and just after the opening of cracks 1, 2 and 3 (at $\varepsilon_{yy} = -1.46\,\%$) is shown in Fig. 6. As an illustration, the location of cracks 2 and 3 is shown by a blue ellipse, and the small dark dots within this ellipse highlight an apparent high equivalent strain due the speckle modifications from cracking. Cracks 2 and 3 occurred at the side of the main deformation bands, but not on these bands. Crack 2 appears to be the closest to the grain boundary, although grain boundaries cannot be positioned precisely enough on top of the image after deformation (Grennerat et al., 2012).

As mentioned in Sect. 2, maps of accumulated strain include some noise, and likely some out-of-plane component of strain. In order to provide a more precise description of the relationship between strain field and crack opening, the following analyses will be performed based on strain-field increments measured during adapted macro-strain increments. This procedure strongly reduces the effect of accumulated noise and out-of-plane strain is negligible during small strain increments.

As a departure point, the strain field during increment of macro-strain between -1.34 and $-1.35\,\%$, just before any visible crack event, is shown in Fig. 7, by both ε_{eq} (grey

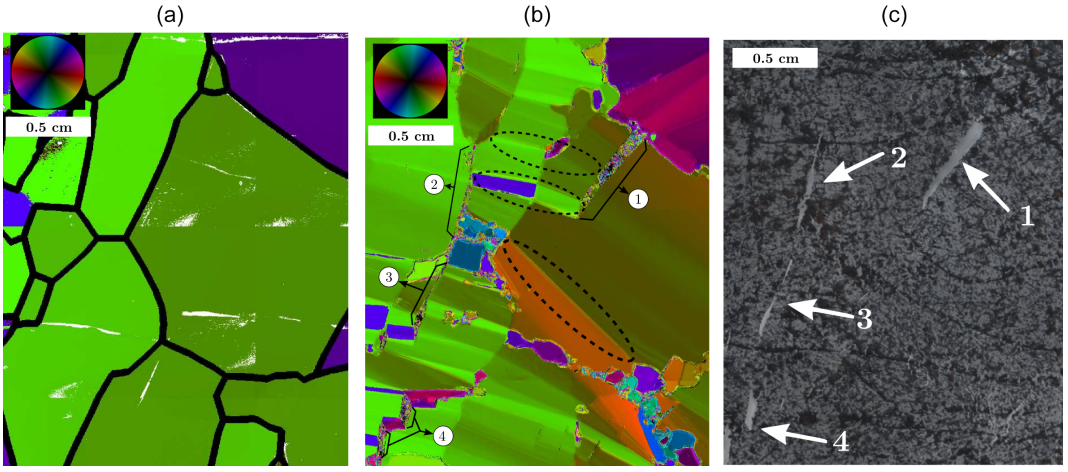

Figure 5. Studied area extracted from the sample of Fig. 3. **(a)** Initial microstructure measured by AITA. The black lines show the superimposed and artificially enlarged grain boundaries. The irregular white lines and small white areas are measurement artifacts. **(b)** Microstructure measured by AITA after deformation. Crack locations are highlighted by black full lines and labeled. Areas where recrystallization by subgrain rotation took place are shown by black dashed ellipses. **(c)** Raw picture of the surface speckle at the end of the test where cracks 1 to 4 can be seen by speckle discontinuities.

color scale) and the projections of the principal strain components (arrows). During this strain increment, strain field is very similar to the one accumulated during the entire experiment before cracking events (Fig. 6, left). Blue ellipses were drawn on the position of future opening of cracks 1, 2 and 3. Local strain within the ellipses is low compared to the one accommodated by the two main bands.

The strain field measured during increments at later steps of the experiment is presented on the different parts of Fig. 8. Cracks 1, 2 and 3 are first observed to open between -1.35 and $-1.46\,\%$ of macro-strain (Fig. 8a). Cracks can be visualized on the speckle as discontinuities, and the DIC calculation provides an apparent strain characterized by a pure extension which provides the main direction of the crack opening. Cracks 1 to 3 could have opened mainly in mode I since no shear component was measured by DIC in the area of crack formation just before the opening (Fig. 7), within the limit of resolution of our observations. During this strain increment, associated with the crack opening, strain is still localized in the nearly horizontal band. The nearly vertical deformation band, which was accommodating a lot of deformation before the cracks start to open, is not active anymore (compare Figs. 6 and 8).

During the next increment (Fig. 8b), cracks continue opening, as illustrated by the tension component evaluated by DIC around the crack sides. From the final microstructure picture (Fig. 6), we see that the top right part of crack 1 is connected to a grain boundary but the bottom part of this crack remains inside the grain, while no clear strain localization can be observed at this position (within our limit of accuracy).

About 30 min later, between macro-strain of -2.40 and $-2.59\,\%$ (Fig. 8c), the strain field evaluation (together with speckle observation) tends to show that cracks 1 and 2 are still expanding when crack 3 remains stable, since DIC calculation shows no more tensile strain components in the area of crack 3.

During this increment, crack 4 appears at the bottom left and two new deformation bands appear at the lower tip of crack 2, and at the bottom tip of crack 3, both being parallel to the main transverse deformation band observed from the beginning of this sequence. These new lines of strain localization end up joining each other and the initial transverse deformation band during the macro-strain interval between -3.12 and $-3.37\,\%$ (Fig. 8d). By looking at the final microstructure (Fig. 5), these new deformation bands appear to be localized in an area where new grains recrystallized. Since we follow the strain field evolution during the test, we are able to verify that the new grains formed after the apparition of the cracks as in Chauve et al. (2015).

At the same time, crack 3 closes, as evidenced by the thinning of the corresponding white zone in the speckle image. Strain in the crack 3 area turns into a pure compressive component (blue arrows, Fig. 8d), which is likely to be responsible for this crack closure. Similarly, during the last increment of deformation (between -5.05 and $-5.50\,\%$ of macro-strain), pure compressive principal strain components are calculated in most of the observed crack discontinuities (Fig. 9). Together with the visual observation of crack evolution on the speckle images, these observations reveal a crack closure mechanism.

During this last increment, strain field is also characterized by several new bands of strain localization in the area (Fig. 9). By observing the final microstructure, we can attribute this strain localization to the formation of high-angle

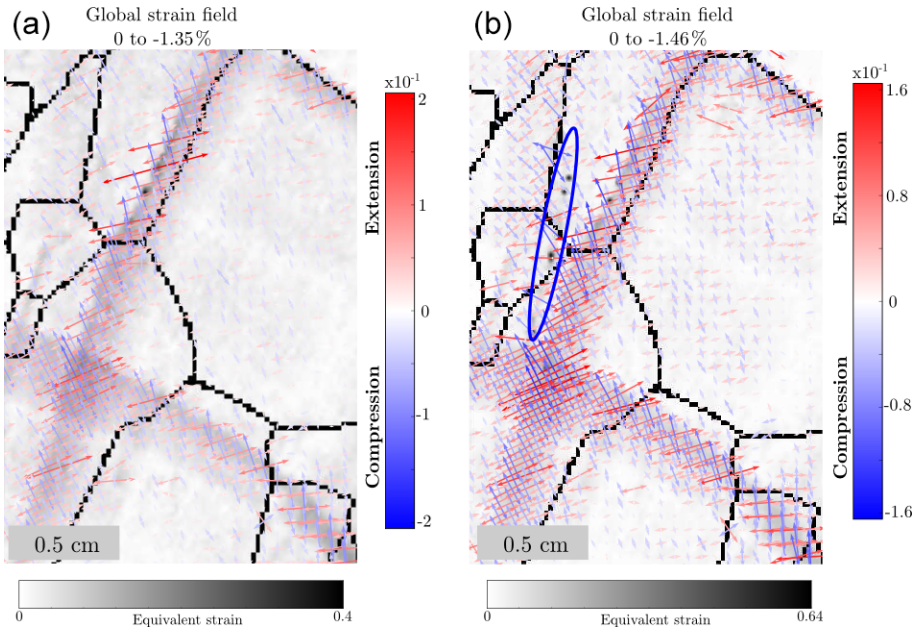

Figure 6. Evaluation of the total accumulated strain field in the focused area from Fig. 3 represented by ε_{eq} and by the principal components. **(a)** Total strain accumulated after $-1.35\,\%$ of macro-strain. **(b)** Total strain accumulated after $-1.46\,\%$ of macro-strain, just after the crack formation. The blue ellipse shows the area of formation of crack 2.

sub-grain boundaries and kink bands. Their likely locations are shown by dashed black ellipses in Figs. 5 and 9 to facilitate the observation. In particular, the two kink bands marked by the top black dashed ellipses seem to be localized at the tips of cracks 2 and 1. Please note that crack 1 bottom tip localized in the grain interior strongly coincides with the edge of a high-angle sub-grain boundary.

To summarize, by measuring the strain field evolution during the onset of tertiary creep, at the ductile-to-brittle transition, we were able to follow crack formation close to grain boundaries and within grain interiors, as well as their consequences on the local strain field. Some cracks appear at the side of high strain localization bands, where stress must have concentrated in "hard" zones for deformation. Following the crack opening, we observe a strong redistribution of the local strain, with the disappearance of one of the major localization band. Additionally, we show that stress concentration at the crack tips can be efficiently relaxed by dynamic recrystallization mechanisms (nucleation and sub-grain boundary formation), and that the stress redistribution induced by crack opening and microstructure changes due to DRX mechanisms can lead to the closure of cracks during the test. The occurrence of dynamic recrystallization mechanisms is here strongly enhanced by the high homologous temperature conditions of the experiment.

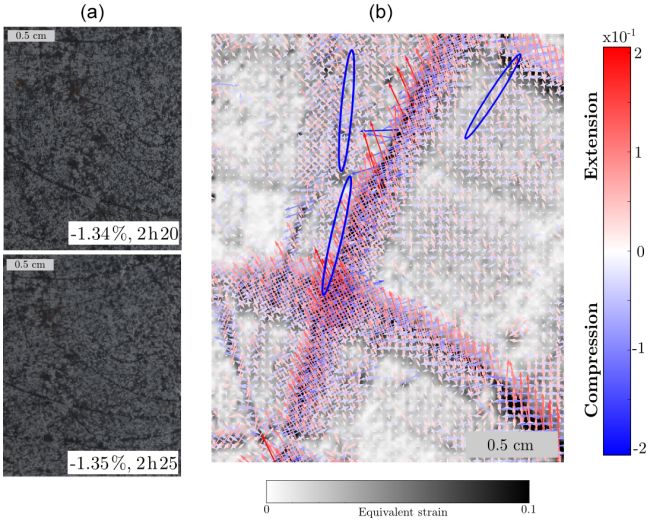

Figure 7. Strain field increment during the 5 min before the apparition of cracks between -1.34 and $-1.35\,\%$ of macroscopic strain. **(a)** Pictures of the speckled surface used for the DIC. **(b)** Principal component of the strain field superimposed on the equivalent strain field (ε_{eq}).

4 Discussion – mechanisms to relax local stress concentration

During compressive tests on an isotropic material, the maximum shear stress occurs at 45° E from the compression direction (Tresca criterion). For material with plastic

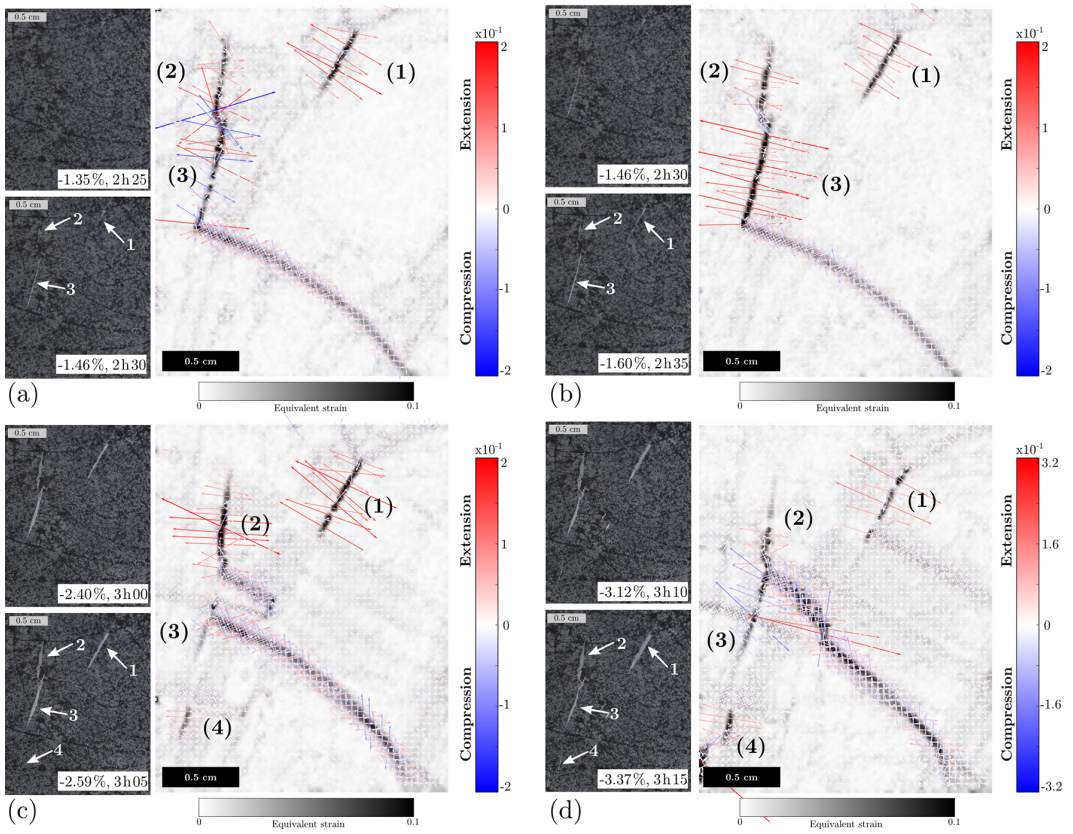

Figure 8. Four steps of 5 min strain field increment during crack opening. **(a, c)** Pictures of the speckled surface used for the DIC. **(b, d)** Principal component of the strain field superimposed on the equivalent strain field. **(a)** Increment between −1.35 and −1.46 %. **(b)** Increment between −1.46 and −1.60 %. **(c)** Increment between −2.40 and −2.59 %. **(d)** Increment between −3.12 and −3.37 %.

anisotropy such as ice, a redistribution of stress is expected to occur which depends on the orientation relationship between grains. Such a redistribution has been simulated by full-field crystal plasticity approaches by Lebensohn et al. (2004) and Grennerat et al. (2012) for instance. Although the stress field is not experimentally accessible so far, these modeling results were validated by a comparison between predicted and measured strain field magnitudes and heterogeneities (Grennerat et al., 2012).

At the onset of tertiary creep in laboratory deformed ice, strain rate increases thanks to accommodating processes. As summarized by Schulson and Duval (2009), depending on the deformation conditions (temperature, imposed stress or imposed strain rate), accommodation can take place through dynamic recrystallization or micro-cracking. To our knowledge, no direct observations exist of the effect of micro-cracking on the redistribution of strain and therefore on local stress relaxation. The results presented here fill this gap by exploring the ductile-to-brittle transition where micro-cracking and plasticity can coexist. Common features with previous observations made by Grennerat et al. (2012) and Chauve et al. (2015) are the strong strain heterogeneities, with local strains more than 10 to 20 times as great as the macroscopic strain. Although influenced by the boundary conditions, grain interactions tend to deviate the strain concentration from the main 45° E directions. While the work of Grennerat et al. (2012) remained in the primary creep regime, and mostly concentrated on sample-scale field characterizations, Chauve et al. (2015) went a step further and found that DRX mechanisms explained the interplay between local changes in microstructure and strain-field evolution. In particular, strain was shown to re-localize close to the newly formed grain boundaries and sub-grain boundaries. This has also been observed in the present study.

Compared with previous works, conditions imposed during the experiment presented here induced local cracking at the onset of tertiary creep (which occurs before 1 % of macro-strain for the sample studied very likely because of the influence of a non-isotropic texture and of a columnar microstructure). Most of the local cracks observed were intragranular. Cracks appeared in areas near strain localization bands, but not within these bands, as evidenced by Fig. 6 and by comparing Figs. 7 and 8a (cracks 1 and 2). These observations highlight the fact that local stresses can be concentrated at the side of high strained region. This can result from strain incompatibilities between regions of different orientations,

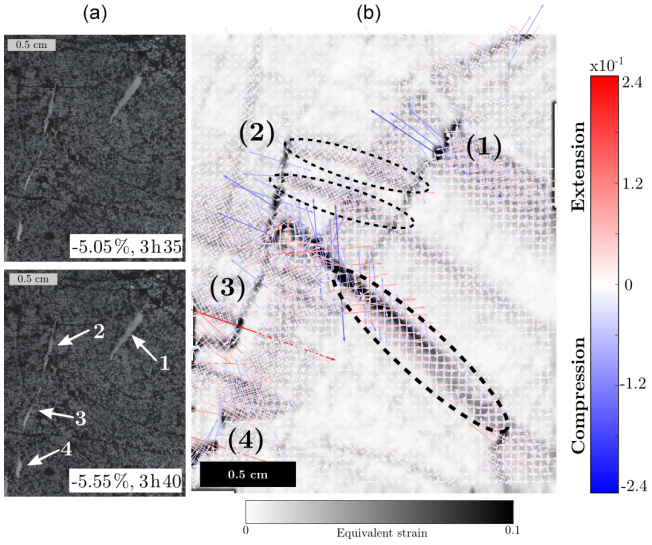

Figure 9. Increment of deformation during the last 5 min of the test (between −5.05 and −5.55 %). Kink band formation (within dashed black ellipses) at the crack tips and crack closure are observed. **(a)** Pictures of the speckled surface used for DIC. **(b)** Principal components of the strain field superimposed on the equivalent strain field.

with regions with locally low Schmid factors (relative to the local stress tensor) behaving as solid inclusions in composite materials. The likely impact of low local Schmid factors might be strengthened by the strong viscoplastic anisotropy of ice that renders some orientations strongly unfavorable for basal dislocation slip.

Crack formation relaxes these high local stresses, and meanwhile, stress concentration is translated at the crack tips. Previous studies on columnar ice performed at higher strain rate ($\dot{\varepsilon} = 4 \times 10^{-3}\,\mathrm{s}^{-1}$) but similar temperature ($T = -10\,^{\circ}\mathrm{C}$; Batto and Schulson, 1993; Iliescu and Schulson, 2004) evidenced the typical mechanism of wing-crack formation at the crack tips. Wing cracks appear as the result of tensile stress concentration at the crack tips and can lead to the overall failure of the sample by propagating through it, or by connecting to other cracks. Recently, a similar mechanism of wing cracks propagation has been characterized by DIC in a soft rock by Nguyen et al. (2011), and they were able to quantify the different fracture modes (opening, closing and shearing) thanks to local strain measurements.

As the experiment presented here is performed in conditions equivalent to a lower strain rate (although through imposed load conditions) compared to Batto and Schulson (1993), the stress concentration at the crack tips is not relaxed by the formation of wing cracks but by plasticity mechanisms in the creep zone at the tip. Dislocations are therefore expected to nucleate and propagate at the crack tips as shown by Rice and Thomson (1974). Recently, Argon (2001) showed that both nucleation of dislocations at the crack tip, and the mobility of the nucleated dislocations come into play to induce the stress relaxation responsible for a crack arrest. Considering the high-temperature conditions of our experiments, the dislocation multiplication leads to dynamic recrystallization mechanisms to occur in the creep zone near crack tips. Indeed, nucleation of new grains is observed very close to the crack tips of cracks 2, 3 and 4 (Fig. 5) and dislocation substructures as sub-grains are formed, for instance around crack tips of cracks 1 and 2 (Fig. 9). These observations reveal that plasticity-driven recrystallization mechanisms are efficient to relax the local tensile stresses initiated at the crack tips.

Local stresses associated with grain interactions during deformation of ice was indeed shown to be strongly heterogeneous, and to be responsible for the initiation of sub-grain boundaries at the end of primary creep (Piazolo et al., 2015). Observation of crack initiation near grain boundaries and within grain interior is another evidence of such local stress concentration.

By following the strain field evolution all along the tests, we observe the closure of some parts of the cracks, in areas where nucleation and sub-grain boundary formation were the most active. Crack closure is evidenced by the representation of principal strains which directions evolve from a tension component to a compressive component that ensures the recovering of continuity (Fig. 8d). In order to obtain a local closure of cracks, the stress field components should be drastically modified, and possibly turn to a compressive component. The new microstructure formed by recrystallization mechanisms must therefore drive a redistribution of the local stress field to enable such a modification, still compatible with the macroscopic stress conditions.

Ductile fracture occurring at elevated temperature in metals can be related to void propagation, growth and coalescence. Recently, Shang et al. (2017) showed that DRX mechanisms induced a softening that reduces the local stress concentration, which serves as the driving force for this void-induced ductile fracture. Similar observations of a ductile-to-brittle transition in Olivine driven by plasticity mechanisms was thoroughly studied by Druiventak et al. (2011). In samples deformed at 20, 300 and 600 °C they observed microcracking at grain boundaries and in the grain interiors, but also arrays of dislocations related to crystal plasticity. Similarly to our observations, at the highest temperature, plasticity took place in the form of strongly misoriented undulatory extinctions (associated with various types of dislocations), deformation lamellae and 3-D dislocation cells inducing strong modifications of the microstructure. Our results therefore present some interest beyond the ice community. Similar procedures could very interestingly be applied to a wide range of materials in order to estimate the role of the level of plastic anisotropy on strain localization and on the efficiency of plasticity-driven recrystallization mechanisms to relax the local stress field at the crack tips.

On top of the mechanical meaning of these observations, we highlight the fact that, since we were able to follow local

crack closure during the test, care must be taken when performing experimental tests in conditions close to the ductile-to-brittle transition (typically at strain rates above $10^{-6}\,s^{-1}$, or compressive stress above 0.9 MPa), and at high temperature. Micro-cracking and DRX mechanisms can influence the local stress relaxation, and therefore the mechanical response, without leaving any track in the final microstructure.

5 Concluding remarks

The present work reveals, for the first time in ice, the evolution of the heterogeneous strain field during the onset of tertiary creep, in conditions where local cracking occurs to relax the local stress field. This observation was made possible by taking advantage of samples with 2-D–1/2 microstructures from which surface observations reflect bulk behavior.

While strain field localizes into bands with a length larger than the grain dimensions, cracks appear to relax stress concentration at the side of the strain localization bands, where deformation by dislocation glide must have been impeded by low local Schmid factor conditions.

Relaxation of the local stress field by crack opening results in a local redistribution of the strain field, as evidenced by the abrupt weakening of some deformation bands after cracking. At the crack tips, where stress concentrates, plasticity-driven dynamic recrystallization mechanisms are observed as new small grains and high-angle sub-grain boundaries in the final microstructure. The new formed boundaries also appear visible on strain field patterns during the test, as new strain concentration areas. While induced by local stress concentration at the crack tip, recrystallization mechanisms in turn generate a stress field redistribution as a result of microstructure modifications. This redistribution is indirectly evidenced by the modification of the measured strain field in the area, but also by the original observation of local crack closure, likely associated with a measured local compressive stress in place of the initial tensile stress responsible for the observed mode I crack opening. To conclude, the main results show that micro-cracking and dynamic recrystallization mechanisms both resulting from a strongly heterogeneous stress field can coexist locally and that these mechanisms are efficient to relax local stresses at the ductile-to-brittle transition. Hence one should be careful when working at the frontiers of this transition since recrystallization can hide local cracking in the final microstructures.

Data availability. Data are accessible by a simple request to the corresponding author.

Author contributions. TC, DG and CL performed the laboratory experiments. DG and TC provided the data treatment. MM and TC analyzed the data and wrote the paper. PV provided some support for the DIC analyses and interpretation.

Competing interests. The authors declare that they have no conflict of interest.

Special issue statement. This article is part of the special issue "Analysis of deformation microstructures and mechanisms on all scales". It is a result of the EGU General Assembly 2016, Vienna, Austria, 17–22 April 2016.

Acknowledgements. Financial support by the French "Agence Nationale de la Recherche" is acknowledged (project DREAM, ANR-13-BS09-0001-01). This work benefited from support from the INSIS and INSU institutes of CNRS. It was supported by a grant from Labex OSUG@2020 (ANR10 LABEX56) and from INP-Grenoble and UJF within the "Grenoble Innovation Recherche AGIR" proposal. Support from the imagery center IRIS of Grenoble-INP is acknowledged. Maurine Montagnat benefited from a visitor research fellowship from WSL (Switzerland) in 2016–2017.

Edited by: Ilka Weikusat
Reviewed by: two anonymous referees

References

Antolovich, S. D. and Armstrong, R. W.: Plastic strain localization in metals: origins and consequences, Prog. Mater. Sci, 59, 1–160, https://doi.org/10.1016/j.pmatsci.2013.06.001, 2014.

Argon, A.: Mechanics and physics of brittle to ductile transitions in fracture, J. Eng. Mater.-T. ASME, 123, 1–11, 2001.

Batto, R. A. and Schulson, E. M.: On the ductile-to-brittle transition in ice under compression, Acta Metall. Mater., 41, 2219–2225, https://doi.org/10.1016/0956-7151(93)90391-5, 1993.

Bons, P. D., Jansen, D., Mundel, F., Bauer, C. C., Binder, T., Eisen, O., Jessell, M. W., Llorens, M.-G., Steinbach, F., Steinhage, D., and Weikusat, I.: Converging flow and anisotropy cause large-scale folding in Greenland's ice sheet, Nat. Commun., 7, 1–6, https://doi.org/10.1038/ncomms11427, 2016.

Chauve, T., Montagnat, M., and Vacher, P.: Strain field evolution during dynamic recrystallization nucleation; A case study on ice, Acta Mater., 101, 116–124, https://doi.org/10.1016/j.actamat.2015.08.033, 2015.

Chauve, T., Montagnat, M., Barou, F., Hidas, K., Tommasi, A., and Mainprice, D.: Investigation of nucleation processes during dynamic recrystallization of ice using cryo-EBSD, Philos. T. R. Soc. A, 375, 1–20, https://doi.org/10.1098/rsta.2015.0345, 2017.

Dahl-Jensen, D., Albert, M. R., Aldahan, A., et al.: Eemian interglacial reconstructed from a Greenland folded ice core, Nature, 493, 489–494, 2013.

Druiventak, A., Trepmann, C. A., Renner, J., and Hanke, K.: Low-temperature plasticity of olivine during high stress deformation of peridotite at lithospheric conditions – An experimental study, Earth Planet. Sc. Lett., 311, 199–211, 2011.

Durand, G., Graner, F., and Weiss, J.: Deformation of grain boundaries in polar ice, Europhys. Lett., 67, 1038, https://doi.org/10.1209/epl/i2004-10139-0, 2004.

Durand, G., Gillet-Chaulet, F., Svensson, A., Gagliardini, O., Kipfstuhl, S., Meyssonnier, J., Parrenin, F., Duval, P., and Dahl-Jensen, D.: Change in ice rheology during climate variations – implications for ice flow modelling and dating of the EPICA Dome C core, Clim. Past, 3, 155–167, https://doi.org/10.5194/cp-3-155-2007, 2007.

Duval, P.: Creep and recrystallization of polycrystalline ice, Bull. Mineral, 102, 80–85, 1979.

Duval, P., Ashby, M., and Anderman, I.: Rate controlling processes in the creep of polycrystalline ice, J. Phys. Chem., 87, 4066–4074, 1983.

Fischer, H., Severinghaus, J., Brook, E., Wolff, E., Albert, M., Alemany, O., Arthern, R., Bentley, C., Blankenship, D., Chappellaz, J., Creyts, T., Dahl-Jensen, D., Dinn, M., Frezzotti, M., Fujita, S., Gallee, H., Hindmarsh, R., Hudspeth, D., Jugie, G., Kawamura, K., Lipenkov, V., Miller, H., Mulvaney, R., Parrenin, F., Pattyn, F., Ritz, C., Schwander, J., Steinhage, D., van Ommen, T., and Wilhelms, F.: Where to find 1.5 million yr old ice for the IPICS "Oldest-Ice" ice core, Clim. Past, 9, 2489–2505, https://doi.org/10.5194/cp-9-2489-2013, 2013.

Grennerat, F., Montagnat, M., Castelnau, O., Vacher, P., Moulinec, H., Suquet, P., and Duval, P.: Experimental characterization of the intragranular strain field in columnar ice during transient creep, Acta Mater., 60, 3655–3666, 2012.

Iliescu, D. and Schulson, E. M.: The brittle compressive failure of fresh-water columnar ice loaded biaxially, Acta Mater., 52, 5723–5735, https://doi.org/10.1016/j.actamat.2004.07.027, 2004.

Jacka, T. H. and Maccagnan, M.: Ice crystallographic and strain rate changes with strain in compression and extension, Cold Reg. Sci. Technol., 8, 269–286, 1984.

Jansen, D., Llorens, M.-G., Westhoff, J., Steinbach, F., Kipfstuhl, S., Bons, P. D., Griera, A., and Weikusat, I.: Small-scale disturbances in the stratigraphy of the NEEM ice core: observations and numerical model simulations, The Cryosphere, 10, 359–370, https://doi.org/10.5194/tc-10-359-2016, 2016.

Lebensohn, R. A., Liu, Y., and Ponte-Castañeda, P.: On the accuracy of the self-consistent approximation for polycrystals: comparison with full-field numerical simulations, Acta Mater., 52, 5347–5361, 2004.

MacGregor, J. A., Fahnestock, M. A., Catania, G. A., Paden, J. D., Prasad Gogineni, S., Young, S. K., Rybarski, S. C., Mabrey, A. N., Wagman, B. M., and Morlighem, M.: Radiostratigraphy and age structure of the Greenland Ice Sheet, J. Geophys. Res.-Earth, 120, 212–241, 2015.

Martínez-Pañeda, E. and Niordson, C. F.: On fracture in finite strain gradient plasticity, Int. J. Plasticity, 80, 154–167, https://doi.org/10.1016/j.ijplas.2015.09.009, 2016.

Montagnat, M., Chauve, T., Barou, F., Tommasi, A., Beausir, B., and Fressengeas, C.: Analysis of dynamic recrystallization of ice from EBSD orientation mapping, Front. Earth Sci., 3, 1–13, https://doi.org/10.3389/feart.2015.00081, 2015.

Nguyen, T. L., Hall, S. A., Vacher, P., and Viggiani, G.: Fracture mechanisms in soft rock: Identification and quantification of evolving displacement discontinuities by extended digital image correlation, Tectonophysics, 503, 117–128, https://doi.org/10.1016/j.tecto.2010.09.024, 2011.

Panton, C. and Karlsson, N. B.: Automated mapping of near bed radio-echo layer disruptions in the Greenland Ice Sheet, Earth Planet. Sc. Lett., 432, 323–331, 2015.

Paterson, W. S. B.: The physics of glaciers, Pergamon, Oxford, 1994.

Peternell, M., Russell-Head, D., and Wilson, C.: A technique for recording polycrystalline structure and orientation during in situ deformation cycles of rock analogues using an automated fabric analyser, J. Microsc., 242, 181–188, 2011.

Piazolo, S., Montagnat, M., Grennerat, F., Moulinec, H., and Wheeler, J.: Effect of local stress heterogeneities on dislocation fields: Examples from transient creep in polycrystalline ice, Acta Mater., 90, 303–309, https://doi.org/10.1016/j.actamat.2015.02.046, 2015.

Ple, O. and Meyssonnier, J.: Preparation and Preliminary Study of Structure-Controlled S2 Columnar Ice, J. Phys. Chem. B, 101, 6118–6122, https://doi.org/10.1021/jp963256t, 1997.

Renshaw, C. E. and Schulson, E. M.: Universal behaviour in compressive failure of brittle materials, Nature, 412, 897–900, https://doi.org/10.1038/35091045, 2001.

Rice, J. R. and Thomson, R.: Ductile versus brittle behaviour of crystals, Philos. Mag., 29, 73–97, 1974.

Schulson, E. and Buck, S.: The ductile-to-brittle transition and ductile failure envelopes of orthotropic ice under biaxial compression, Acta Metall. Mater., 43, 3661–3668, 1995.

Schulson, E. M. and Duval, P.: Creep and Fracture of Ice, Cambridge University Press, https://doi.org/10.1017/CBO9780511581397, 2009.

Schulson, E. M., Lim, P. N., and Lee, R. W.: A brittle to ductile transition in ice under tension, Philos. Mag. A, 49, 353–363, https://doi.org/10.1080/01418618408233279, 1984.

Shang, X., Cui, Z., and Fu, M. W.: Dynamic recrystallization based ductile fracture modeling in hot working of metallic materials, Int. J. Plasticity, 95, 105–122, https://doi.org/10.1016/j.ijplas.2017.04.002, 2017.

Snyder, S. A., Schulson, E. M., and Renshaw, C. E.: Effects of prestrain on the ductile-to-brittle transition of ice, Acta Mater,, 108, 110–127, https://doi.org/10.1016/j.actamat.2016.01.062, 2016.

Tommasi, A., Knoll, M., Vauchez, A., Signorelli, J., Thoraval, C., and Logé, R.: Structural reactivation in plate tectonics controlled by olivine crystal anisotropy, Nat. Geosci., 2, 423–427, https://doi.org/10.1038/ngeo528, 2009.

Vacher, P., Dumoulin, S., Morestin, F., and Mguil-Touchal, S.: Bidimensional strain measurement using digital images, P. I. Mech. Eng. C-J. Mec., 213, 811–817, 1999.

Vauchez, A., Tommasi, A., and Mainprice, D.: Faults (shear zones) in the Earth's mantle, Tectonophysics, 558, 1–27, 2012.

Weiss, J. and Schulson, E. M.: Grain-boundary sliding and crack nucleation in ice, Philos. Mag. A, 80, 279–300, https://doi.org/10.1080/01418610008212053, 2000.

Wilson, C., Russell-Head, D., and Sim, H.: The application of an automated fabric analyzer system to the textural evolution of folded ice layers in shear zones, Ann. Glaciol., 37, 7–17, 2003.